Synchronization of Dissipative Nosé–Hoover Systems: Circuit Implementation

Rending LU [1], Hayder NATIQ [2], Ahmed M. Ali ALI [3,4], Hamid Reza ABDOLMOHAMMADI [5], Sajad JAFARI [6,7]

[1] School of Electronic Engineering, Changzhou College of Information Technology, 213164, China
[2] Dept. of Computer Technology Engineering, College of Information Technology, Imam Ja'afar Al-Sadiq University, Baghdad, Iraq
[3] Dept. of Electronics Techniques, Babylon Technical Institute, Al-Furat Al-Awsat Technical University, Babylon, Iraq
[4] Al-Mustaqbal University College, Babylon, 51001, Iraq
[5] Electrical and Computer Engineering Group, Golpayegan College of Engineering, Isfahan University of Technology, Golpayegan, 87717-67498, Iran
[6] Health Technology Research Institute, Amirkabir University of Technology (Tehran Polytechnic), Tehran, Iran
[7] Dept. of Biomedical Engineering, Amirkabir University of Technology (Tehran Polytechnic), Tehran, Iran

36429720@qq.com, haydernatiq86@gmail.com, Ahmed.ali@atu.edu.iq, abdolmohammadi@iut.ac.ir, sajadjafari83@gmail.com

Submitted July 27, 2023 / Accepted September 4, 2023 / Online first October 30, 2023

Abstract. *The synchronization of dynamical systems has been extensively studied across various scientific disciplines, including secure communication, providing insights into the collective behavior of complex systems. This paper investigated the synchronization of diffusively coupled dissipative Nosé-Hoover (DNH) systems analytically and experimentally. This system exhibits a variety of fascinating dynamical phenomena, including multistable or monostable chaotic solutions and attractive torus. The DNH circuit is implemented in OrCAD–PSpice, focusing on chaotic dynamics. The DNH system is thus said to be diffusively coupled by considering a passive resistor to link the corresponding states of two DNH circuits. The coupling scheme and strength (resistor value) under which two circuits can be synchronized are attained using the master stability function method and are then confirmed by computing the synchronization error. The correlation of coupled circuits' outputs (time evolutions) demonstrates complete synchronization, which is consistent with the analytical and experimental results.*

Keywords

Synchronization, dissipative Nosé–Hoover system, master stability function, chaotic circuit

1. Introduction

The deliberate use of nonlinear elements in chaotic circuit design results in circuits that behave chaotically [1–3]. Chaotic circuit design embraces the inherent unpredictability and complexity of chaotic systems as opposed to traditional circuit design, which seeks steady and predictable performance [4], [5]. These circuits are useful for many different applications, including cryptography, secure communications, and random number generation, since they produce complex and seemingly random waveforms [6–8]. For instance, image encryption is currently a prominent area of research that can be effectively implemented using chaotic systems [9–11]. Therefore, many chaotic systems have been designed and analogously implemented in the literature. Chua's system and its variations are the most famous chaotic circuits that have been studied in different fields. For instance, the hidden attractors of Chua's circuit were investigated in [12]. Introducing the fractional-order Chua's circuit with modifications was the subject of the study in [13]. A simplified version of Chua's circuit was introduced in [14], and many studies have been conducted on proposing or investigating memristor-based Chua's circuit [15–17]. In addition to Chua's system, different chaotic circuits with their corresponding mathematical models have been proposed. For example, a new circuit with multiple memristors was designed in [18]. A chaotic circuit with one stable equilibrium point is presented in [19]. Using five state variables, in [20], a novel circuit was designed with the ability to exhibit extreme multistability. The hardware implementation of the memristive Hodgkin–Huxley neuron model was proposed in [21], and similarly, using local active memristors, another neuromorphic circuit was designed in [22].

Synchronization of chaotic oscillators refers to the phenomena in which two or more chaotic oscillators attain coordinated behavior due to their nonlinear dynamics and unpredictability. It entails adjusting the states and dynamics of the

DOI: 10.13164/re.2023.0511

oscillators so that they become correlated and exhibit similar patterns over time. Complete synchronization [23], imperfect synchronization [23], generalized synchronization [24], cluster synchronization [25], phase synchronization [26], lag synchronization [27], and partial synchronization [28] are all different synchronization aspects. Complete synchronization, the most well-known and important type of synchronization, is the state in which two or more chaotic oscillators exhibit identical behavior, with all of their state variables converging to the same values and their trajectories nearly overlapping [29], [30]. The chaotic systems effectively operate as a single system, with their dynamics precisely coordinated, offering applications in areas such as secure communications, where they can be utilized for encryption purposes [31–33] and neuroscience to study the brain's function [34–37]. The synchronization of chaotic circuits has gained significant attention due to its potential applications in various fields, particularly secure communication and information transmission. Complete synchronization can be assessed through experiments and master stability function (MSF). The MSF, coined by Pecora and Carroll in 1998 [38], is a mathematical tool used to analyze the stability of synchronized states in complex networks. It provides a criterion to determine under what conditions a network of coupled dynamical systems can achieve and maintain synchronization. Using experimental or MSF-based approaches, the synchronization of different chaotic systems and circuits has been taken into account. For example, the synchronization of two coupled Chua's circuits was investigated in [39] using the MSF-based analysis. In this study, a passive resistor was considered to link two corresponding states of circuits. The complete synchronization of two or more diffusively coupled elegant circuits, equivalent to linking corresponding states by a resistor, was studied using both experiments and the MSF technique [40]. In another study detailed in [41], the extended MSF method is used to examine the stability of synchronization in a network of nearly identical Chua's circuits. As a theoretical framework to investigate cluster synchronization, the MSF-based analysis was used to confirm the experimental results in a network of neuronal circuits with gap junctions as the connection between the corresponding states, addressed in [42]. In another study [43], iter-layer synchronization of a two-layer network of electronic circuits is explored using experiments and the MSF method. The multiplex network of Chus's circuits was also investigated in [44], considering both resistors and capacitors as static and dynamic diffusive couplings.

This paper investigates the synchronization of two coupled dissipative Nosé–Hoover (DNH) systems in both experimental and analytical approaches. The Nosé–Hoover system, known as the Sprott A system, is a third-case conservative system based on the categories defined in [45]. However, the dissipative version of the Nosé–Hoover system was proposed in [46]. More details about the definition, dynamics, and importance of the DNH system are provided in Sec. 2. In Sec. 3, the circuit implementation of the DNH system is presented. The MSF-based analysis to obtain the necessary synchronization criteria, i.e., the coupling scheme and coupling strength, is performed mathematically in Sec. 4. Section 5 includes the results of the MSF-based approach and the synchronization error as a numerical tool to evaluate the MSF-based results. Moreover, the circuit implementation in the synchronous state is given in Sec. 5. To conclude the paper, Section 6 highlights the findings by summing up the results.

2. Definition

The Nosé–Hoover system is generally described by the following equations:

$$\begin{aligned} \frac{\mathrm{d}x}{\mathrm{d}t} &= y, \\ \frac{\mathrm{d}y}{\mathrm{d}t} &= -x - yz, \\ \frac{\mathrm{d}z}{\mathrm{d}t} &= y^2 - a. \end{aligned} \tag{1}$$

In the equations above, a is the control parameter. The term yz functions as a thermostat in System (1) by interpreting. y^2 as the normalized temperature at each instant. Since $\langle \frac{\partial \dot{x}}{\partial x} + \frac{\partial \dot{y}}{\partial y} + \frac{\partial \dot{z}}{\partial z} \rangle$, where $\langle ... \rangle$ denotes averaging over a time duration after removing transients, and $\langle z \rangle = 0$, based on the previously reported results, the Nosé–Hoover system is recognized as a well-known instance of conservative systems. Additionally, this system exhibits a chaotic sea in coexistence with nested conservative tori. The Nosé–Hoover system, also known as the Nosé–Hoover thermostat, is important since it describes how a thermostat behaves at a specific temperature. A damping term $+bz$ added to the third equation of System (1) has recently been demonstrated to increase the system's dissipativeness significantly [46]. The damped or dissipative system is then defined in further detail as follows:

$$\begin{aligned} \frac{\mathrm{d}x}{\mathrm{d}t} &= y, \\ \frac{\mathrm{d}y}{\mathrm{d}t} &= -x - yz, \\ \frac{\mathrm{d}z}{\mathrm{d}t} &= y^2 - a + bz. \end{aligned} \tag{2}$$

Here b is a control parameter with a real and positive value. This newly defined system is considered the DNH system. Letting b valued as a small positive value like 0.3, Figure 1 shows the rich dynamical properties of System (2), taking a gradually increases from 1.5 to 10. To obtain the bifurcation diagram and the Lyapunov exponents (LEs) spectra $x(0) = -0.5$, $y(0) = 0$, and $z(0) = 0$ are used. Moreover, the LEs spectra are calculated employing the Wolf algorithm presented in [47]. Figure 1 shows System (2) exhibits attracting torus for $2.078 \leq a \leq 2.452$, $6.787 \leq a \leq 8.062$, and $8.266 \leq a \leq 8.776$ (with many periodic windows), chaotic solutions for $2.639 \leq a \leq 2.741$, $2.996 \leq a \leq 3.03$, $3.268 \leq a \leq 4.186$, and $4.305 \leq a \leq 5.019$, and periodic orbits for the rest of the studied range of parameter a. Many periodic windows within the chaotic and torus zones can be

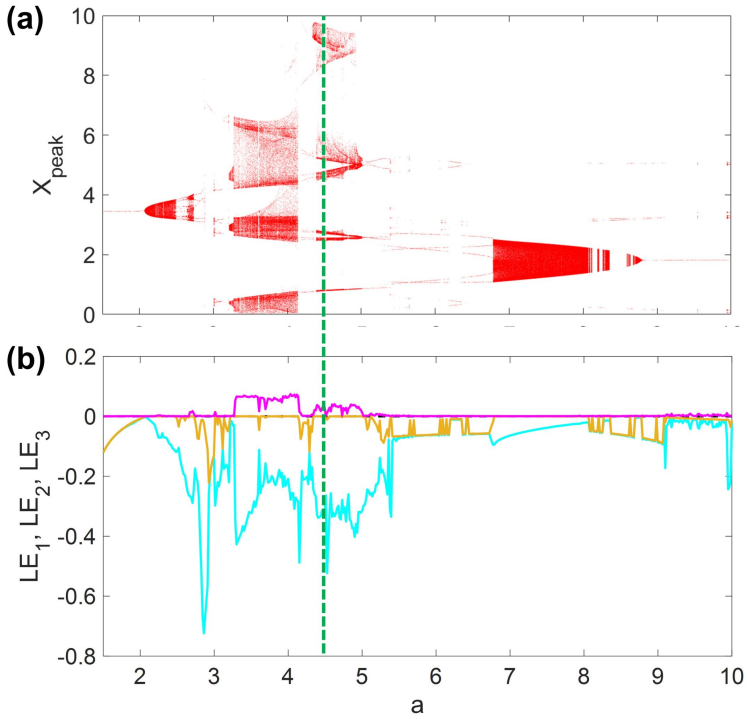

Fig. 1. Various dynamical behavior of the DNH system in terms of (a) the bifurcation diagram and (b) the LEs spectra. Here $b = 0.3$ and $x(0) = -0.5$, and $y(0) = z(0) = 0$ are considered.

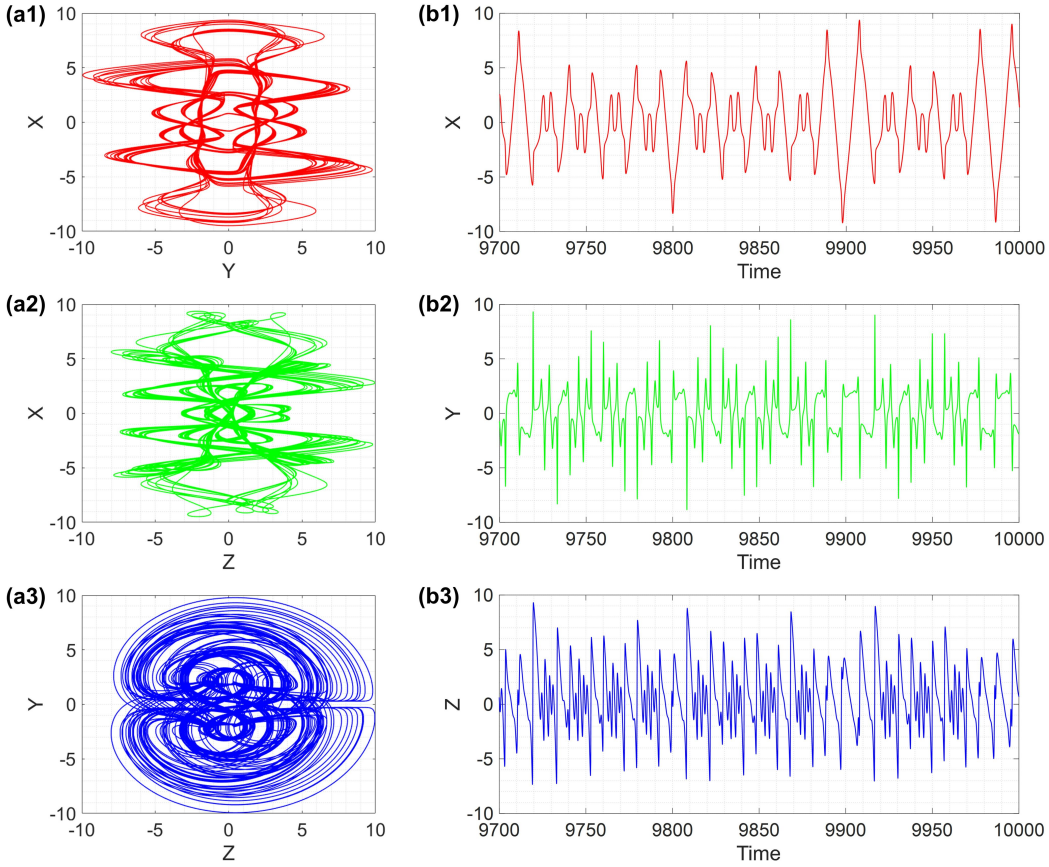

Fig. 2. The chaotic dynamic of the DNH system represented as (a1)–(a3) phase portraits in $x - y$, $x - z$, and $y - z$ plane and (b1)–(b3) time series of variables x, y, and z. Here $a = 4.5$, $b = 0.3$ and $x(0) = -0.5$, and $y(0) = z(0) = 0$ are considered.

detected, while exterior and interior crises can also be found at critical values of a where the system's dynamic alters, or the attractor volume suddenly increases.

Taking the parameter $a = 4.5$, which is in the chaotic area of Fig. 1 and marked with the green dashed line, the phase portraits of the system trajectory in $x - y$, $x - z$, and $y - z$ plane is displayed in Fig. 2 alongside the time series of the variables x, y, and z. Since System (2) continues to be impacted by the transformation $(x, y, z) \to (-x, -y, z)$, the attractor in Fig. 2 is symmetric with regard to the $x - y$ plane. Moreover, the LEs of the attractor are $LE_1 = -0.325$, $LE_2 = 0$, and $LE_3 = 0.025$, ensuring that the observed solution is chaotic.

3. Circuit Realization

The equivalent circuit definition of System (2) can be expressed as:

$$\begin{aligned}
\frac{\mathrm{d}x(t)}{\mathrm{d}t} &= \frac{1}{R_1C_1}y(t),\\
\frac{\mathrm{d}y(t)}{\mathrm{d}t} &= -\frac{1}{R_2C_2}x(t) - \frac{1}{10R_3C_2}y(t)z(t),\\
\frac{\mathrm{d}z(t)}{\mathrm{d}t} &= \frac{1}{10R_4C_3}y(t)^2 - \frac{1}{R_5C_3}V_\mathrm{p}(t) + \frac{1}{R_6C_3}z(t).
\end{aligned} \tag{3}$$

Thus, it reads:

$$\begin{aligned}
x(t) &= -\frac{1}{R_1C_1}\int_0^t -y(t)\mathrm{d}t + x_0,\\
y(t) &= -\frac{1}{R_2C_2}\int_0^t x(t)\mathrm{d}t\\
&\quad - \frac{1}{10R_3C_2}\int_0^t y(t)\times z(t)\mathrm{d}t + y_0,\\
z(t) &= -\frac{1}{10R_4C_3}\int_0^t -y(t)\times y(t)\mathrm{d}t\\
&\quad - \frac{1}{R_5C_3}\int_0^t V_\mathrm{p}(t) - \frac{1}{R_6C_3}\int_0^t -z(t)\mathrm{d}t + z_0.
\end{aligned} \tag{4}$$

Using the three circuit elements, namely resistors, capacitors, and opamps, Figure 3 represents the circuit schematic of the DNH system in the OrCAD–PSpice environment. Assuming $R_1 = 30\,\mathrm{k\Omega}$ and $C_1 = C_2 = C_3 = 10\,\mathrm{nF}$, other values of the main circuits in Fig. 3 (mentioned in System (3) can be solved as $R_2 = 30\,\mathrm{k\Omega}$, $R_3 = R_4 = 3\,\mathrm{k\Omega}$, $R_5 = R_6 = 100\,\mathrm{k\Omega}$. The resistors in the subcircuits of Fig. 3 are valued as $R = 100\,\mathrm{k\Omega}$, which are adjustable.

The circuit output, i.e., phase portraits in the $x-y$, $x-z$, and $y - z$ plane, as well as the time series of variables x, y, and z, is demonstrated in Fig. 4 using the mentioned circuit parameter values which is resemble the results of implementation in MATLAB software (shown in Fig. 2). It should be noted that the circuit is solved for 1000 milliseconds with the maximum time step of $\Delta t = 0.00001$ in OrCAD–PSpice, while in MATLAB, the fourth-order Runge–Kutta algorithm is used to solve the system's set of equations with the time step of $\Delta t = 0.001$ for 10000 milliseconds. Also, the same initial conditions, i.e., $x(0) = -0.5$, $y(0) = 0$, and $z(0) = 0$, is considered in circuit implementation.

4. Synchronization Analysis Based on MSF

Considering a system of two coupled DNH systems coupled through a passive resistor, which can be described as a diffusive term applied to connect state(s)/variable(s), the following equations can be defined for every possible condition:

$$\begin{aligned}
\frac{\mathrm{d}x_1}{\mathrm{d}t} &= y_1 +\\
&\quad \sigma_{xx}(x_2 - x_1) + \sigma_{yx}(y_2 - y_1) + \sigma_{zx}(z_2 - z_1),\\
\frac{\mathrm{d}y_1}{\mathrm{d}t} &= -x_1 - y_1z_1 +\\
&\quad \sigma_{xy}(x_2 - x_1) + \sigma_{yy}(y_2 - y_1) + \sigma_{zy}(z_2 - z_1),\\
\frac{\mathrm{d}z_1}{\mathrm{d}t} &= y_1^2 - a + bz_1 +\\
&\quad \sigma_{xz}(x_2 - x_1) + \sigma_{yz}(y_2 - y_1) + \sigma_{zz}(z_2 - z_1),\\
\frac{\mathrm{d}x_2}{\mathrm{d}t} &= y_2 +\\
&\quad \sigma_{xx}(x_1 - x_2) + \sigma_{yx}(y_1 - y_2) + \sigma_{zx}(z_1 - z_2),\\
\frac{\mathrm{d}y_2}{\mathrm{d}t} &= -x_2 - y_2z_2 +\\
&\quad \sigma_{xy}(x_1 - x_2) + \sigma_{yy}(y_1 - y_2) + \sigma_{zy}(z_1 - z_2),\\
\frac{\mathrm{d}z_2}{\mathrm{d}t} &= y_2^2 - a + bz_2 +\\
&\quad \sigma_{xz}(x_1 - x_2) + \sigma_{yz}(y_1 - y_2) + \sigma_{zz}(z_1 - z_2).
\end{aligned} \tag{5}$$

To investigate the case wherein two DNH systems coordinate their temporal behavior to the same chaotic dynamics shown in Figs. 2 and 4, the MSF approach is used. The MSF method is a mathematical tool proposed by Pecora and Carroll in 1998 [38], allowing to obtain the necessary conditions under which N coupled oscillators synchronize.

Letting v be a vector of states ($v = [x, y, z]$) and $F(v)$ describes the velocity field or, in other words, the dynamics of the system ($F(v) = [\frac{\mathrm{dx}}{\mathrm{d}t}, \frac{\mathrm{dy}}{\mathrm{d}t}, \frac{\mathrm{dz}}{\mathrm{d}t}]$), System (5) can be generally written as:

$$\frac{\mathrm{d}v_i}{\mathrm{d}t} = F(v_i) - \sigma\sum_{j=1}^{N} A_{ij}H(v_j) \tag{6}$$

in which H is the coupling function that specifies which variable the diffusive function is in terms of and which equation it is added to. Thus, it is basically a $d \times d$ matrix, where d is the dimension of the studied system (here, $d = 3$). A is the coupling matrix where $\sum_{j=1}^{N} A_{ij} = 0$ for each row of the matrix belonging to the node i, where $i = 1, 2$. This matrix determines which nodes are connected through a link. Consequently, $A_{ij} = 1$ means there is a link between nodes i and j, while $A_{ii} = \alpha_i$, where α_i is the degree of the node i.

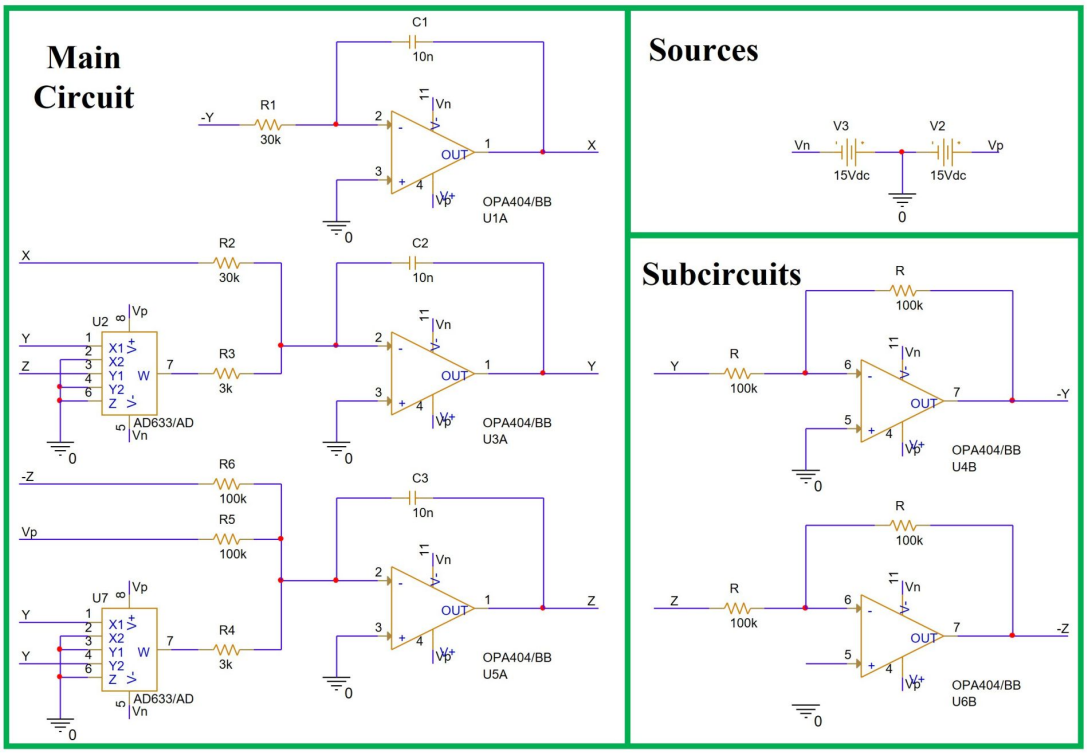

Fig. 3. The circuit implementation of the DNH system in the OrCAD–PSpice environment.

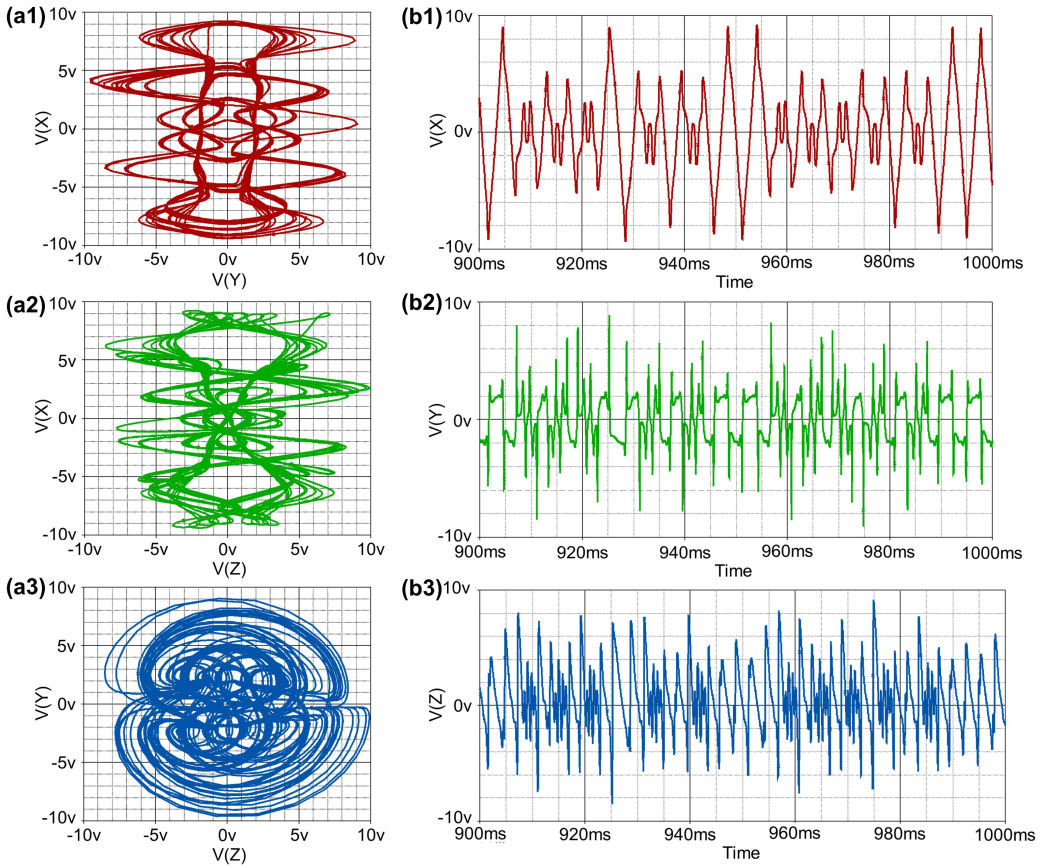

Fig. 4. The output of the DNH system analog circuit represented as (a1)–(a3) phase portraits in $x-y$, $x-z$, and $y-z$ plane and (b1)–(b3) time series of variables x, y, and z. Here $a = 4.5$, $b = 0.3$ and $x(0) = -0.5$, and $y(0) = z(0) = 0$ are considered.

Also, N is the number of interconnected systems (here, $N = 2$), and σ is the coupling parameter determining the strength of the connection between two nodes. It should be noted that, here, $\sigma = \begin{bmatrix} \sigma_{xx} & \sigma_{yx} & \sigma_{zx} \\ \sigma_{xy} & \sigma_{yy} & \sigma_{zy} \\ \sigma_{xz} & \sigma_{yz} & \sigma_{zz} \end{bmatrix}$ with the similar notation used in System (5).

In the case where all systems behave synchronously in time, the diffusive term disappears from (6) since all states are equal, i.e., $v_1(t) = v_2(t) = v(t)$. This means that each node pursues the dynamics of a single system (defined by System (2)). This synchronous state needs to be resilient to local disturbance if it is to be considered stable. Given that δv is the local disturbance added to the synchronous state, where $\delta v(t) = v_i(t) - v(t)$, the dynamics of the variational equations can be expressed as:

$$\frac{\mathrm{d}\delta v_i}{\mathrm{d}t} = JF(v)\delta v_i - \sigma \sum_{j=1}^{N} A_{ij} JH(v)\delta v_j \tag{7}$$

where JF and JH are both $d \times d$ Jacobian matrices corresponding to the functions F and H evaluated at the synchronization state or $v(t)$. Here, $JF(v)$ can be obtained via $\begin{bmatrix} 0 & 1 & 0 \\ -1 & -z & -y \\ 0 & 2y & b \end{bmatrix}$.

Assuming A as a diagonalizable matrix with eigenvalues λ_i, where $0 = \lambda_1 < \lambda_2 < \ldots < \lambda_N$, and matrix Q containing the eigenvectors of matrix A as its columns, the transformation $\zeta = Q^{-1}\delta v$ results in a new set of linearized equations by describing A by its eigenvalues as follows:

$$\frac{d\zeta_i}{\mathrm{d}t} = [JF(v) - \sigma\lambda_i JH(v)]\zeta_i. \tag{8}$$

Considering K as the normalized coupling parameter where $K = \sigma\lambda$, (8) can be rewritten in its generic form as below:

$$\frac{d\zeta}{\mathrm{d}t} = [JF(v) - KJH(v)]\zeta. \tag{9}$$

Due to the diffusive nature of the couplings in this study, where $d = 3$, $N = 2$ and $\lambda_2 = 2$, $JH(v)$ determines where to put the passive resistor in the corresponding circuit. More clearly, based on $JH(v)$ different configurations can be studied, which are noted in Tab. 1. The largest LE calculated from System (9) is the MSF (Ψ), where $\Psi < 0$ reveals that the local disturbance can exponentially dwindle; therefore, the synchronous solution is stable.

Notation	Coupling scheme	Coupling parameters in System (5)
$1 \to 1$	$JH(v) = \begin{bmatrix} 1 & 0 & 0 \\ 0 & 0 & 0 \\ 0 & 0 & 0 \end{bmatrix}$	$\sigma = \begin{bmatrix} K/2 & 0 & 0 \\ 0 & 0 & 0 \\ 0 & 0 & 0 \end{bmatrix}$
$2 \to 1$	$JH(v) = \begin{bmatrix} 0 & 1 & 0 \\ 0 & 0 & 0 \\ 0 & 0 & 0 \end{bmatrix}$	$\sigma = \begin{bmatrix} 0 & K/2 & 0 \\ 0 & 0 & 0 \\ 0 & 0 & 0 \end{bmatrix}$
$3 \to 1$	$JH(v) = \begin{bmatrix} 0 & 0 & 1 \\ 0 & 0 & 0 \\ 0 & 0 & 0 \end{bmatrix}$	$\sigma = \begin{bmatrix} 0 & 0 & K/2 \\ 0 & 0 & 0 \\ 0 & 0 & 0 \end{bmatrix}$
$1 \to 2$	$JH(v) = \begin{bmatrix} 0 & 0 & 0 \\ 1 & 0 & 0 \\ 0 & 0 & 0 \end{bmatrix}$	$\sigma = \begin{bmatrix} 0 & 0 & 0 \\ K/2 & 0 & 0 \\ 0 & 0 & 0 \end{bmatrix}$
$2 \to 2$	$JH(v) = \begin{bmatrix} 0 & 0 & 0 \\ 0 & 1 & 0 \\ 0 & 0 & 0 \end{bmatrix}$	$\sigma = \begin{bmatrix} 0 & 0 & 0 \\ 0 & K/2 & 0 \\ 0 & 0 & 0 \end{bmatrix}$
$3 \to 2$	$JH(v) = \begin{bmatrix} 0 & 0 & 0 \\ 0 & 0 & 1 \\ 0 & 0 & 0 \end{bmatrix}$	$\sigma = \begin{bmatrix} 0 & 0 & 0 \\ 0 & 0 & K/2 \\ 0 & 0 & 0 \end{bmatrix}$
$1 \to 3$	$JH(v) = \begin{bmatrix} 0 & 0 & 0 \\ 0 & 0 & 0 \\ 1 & 0 & 0 \end{bmatrix}$	$\sigma = \begin{bmatrix} 0 & 0 & 0 \\ 0 & 0 & 0 \\ K/2 & 0 & 0 \end{bmatrix}$
$2 \to 3$	$JH(v) = \begin{bmatrix} 0 & 0 & 0 \\ 0 & 0 & 0 \\ 0 & 1 & 0 \end{bmatrix}$	$\sigma = \begin{bmatrix} 0 & 0 & 0 \\ 0 & 0 & 0 \\ 0 & K/2 & 0 \end{bmatrix}$
$3 \to 3$	$JH(v) = \begin{bmatrix} 0 & 0 & 0 \\ 0 & 0 & 0 \\ 0 & 0 & 1 \end{bmatrix}$	$\sigma = \begin{bmatrix} 0 & 0 & 0 \\ 0 & 0 & 0 \\ 0 & 0 & K/2 \end{bmatrix}$

Tab. 1. Different notations to study the synchronization of two coupled DNH systems.

5. Results

Performing the Lyapunov analysis on System (9) concerning the changing in the value of the K parameters, the MSF of all cases noted in Tab. 1 is obtained and shown in Fig. 5. As the results show, the coupling term, which, in fact, acts as linear feedback, can lead to the synchronization only for cases $1 \to 1$, $2 \to 2$, and $3 \to 3$. More clearly, the following networks can achieve synchrony accordingly:

$$\begin{cases} \dfrac{\mathrm{d}x_1}{\mathrm{d}t} = y_1 + \dfrac{K}{2}(x_2 - x_1), \\ \dfrac{\mathrm{d}y_1}{\mathrm{d}t} = -x_1 - y_1 z_1, \\ \dfrac{\mathrm{d}z_1}{\mathrm{d}t} = y_1^2 - a + b z_1, \\ \dfrac{\mathrm{d}x_2}{\mathrm{d}t} = y_2 + \dfrac{K}{2}(x_1 - x_2), \\ \dfrac{\mathrm{d}y_2}{\mathrm{d}t} = -x_2 - y_2 z_2, \\ \dfrac{\mathrm{d}z_2}{\mathrm{d}t} = y_2^2 - a + b z_2, \end{cases} \tag{10}$$

$$\begin{cases} \dfrac{\mathrm{d}x_1}{\mathrm{d}t} = y_1, \\ \dfrac{\mathrm{d}y_1}{\mathrm{d}t} = -x_1 - y_1 z_1 + \dfrac{K}{2}(y_2 - y_1), \\ \dfrac{\mathrm{d}z_1}{\mathrm{d}t} = y_1^2 - a + b z_1, \\ \dfrac{\mathrm{d}x_2}{\mathrm{d}t} = y_2, \\ \dfrac{\mathrm{d}y_2}{\mathrm{d}t} = -x_2 - y_2 z_2 + \dfrac{K}{2}(y_1 - y_2), \\ \dfrac{\mathrm{d}z_2}{\mathrm{d}t} = y_2^2 - a + b z_2, \end{cases} \tag{11}$$

$$\begin{cases} \dfrac{\mathrm{d}x_1}{\mathrm{d}t} &= y_1, \\ \dfrac{\mathrm{d}y_1}{\mathrm{d}t} &= -x_1 - y_1 z_1, \\ \dfrac{\mathrm{d}z_1}{\mathrm{d}t} &= y_1^2 - a + bz_1 + \dfrac{K}{2}(z_2 - z_1), \\ \dfrac{\mathrm{d}x_2}{\mathrm{d}t} &= y_2, \\ \dfrac{\mathrm{d}y_2}{\mathrm{d}t} &= -x_2 - y_2 z_2, \\ \dfrac{\mathrm{d}z_2}{\mathrm{d}t} &= y_2^2 - a + bz_2 + \dfrac{K}{2}(z_1 - z_2). \end{cases} \tag{12}$$

Figure 5 shows that System (10) synchronizes when $2.8 < K < 5.3$ since, in this range of K values, Ψ is negative. Thus, two zero crossing point is observed, and according to the notation in [48], this type of MSF can be classified in the class Γ_2. However, for System (11), three crossing points can be detected in the MSF diagram, which are $K = 0.22, 0.36,$ and 0.54. Here, Ψ is negative for $0.22 < K < 0.36$ and $K > 0.54$. Therefore, this type of MSF is classified in the class Γ_3. System (12) also can be categorized in class Γ_1 since only one zero crossing point can be identified in the MSF diagaram, and $\Psi < 0$ can be seen for $K > 0.5$. All other coupling schemes do not allow for synchronization, and thus, they are categorized in the class Γ_0. For further analysis and to confirm the results reported by the MSF calculations, Systems (10)–(12), which are able to synchronize for certain values of parameter K, are used to calculate the synchronization error (E_{avg}). Synchronization error is a numerical approach that can show the regions of coupling parameters leading to synchronization states since it becomes zero when systems become fully synchronized. The synchronization error is computed via the following relation:

$$E_{\mathrm{avg}} = \lim_{T\to\mathrm{inf}} \frac{1}{T} \int_0^T \sqrt{(x_2 - x_1)^2 + (y_2 - y_1)^2 + (z_2 - z_1)^2} \tag{13}$$

where T is the run-time after removing the transients. Figure 6 shows the synchronization error of two coupled DNH systems for cases $1 \to 1$ (System (10)), $2 \to 2$ (System (11)), and $3 \to 3$ (System (12)).

The results shown in Fig. 6 align with those observed in Fig. 5, and thus, it is expected to obtain synchronous temporal behaviors when two DNH circuits are coupled through a resistor in $1 \to 1$, $2 \to 2$, $3 \to 3$ coupling schemes (shown in Fig. 7). According to Figs. 5 and 6, the circuits are expected to synchronize for $K = 4$ in $1 \to 1$ and in $1 \to 1$ and $3 \to 3$ coupling schemes $K = 1$ is enough to synchronize the coupled DNH systems. Therefore, in $1 \to 1$ configuration, $R_7 = R_8 = 120\,\mathrm{k\Omega}$ (for $K = 4$), and in both $2 \to 2$ and $3 \to 3$ schemes, $R_7 = R_8 = 30\,\mathrm{k\Omega}$ (for $K = 1$) are considered to model the resistors and the linear feedback between the circuit states.

Figure 8 shows that the circuits designed in Fig. 7 achieve synchrony after passing 5000 milliseconds, while in MATLAB software, the results are demonstrated for 10000 milliseconds. Moreover, it can be seen that the circuits' outputs are the same as the time series in Figs. 2 and 4. This means that the system's behavior in the synchronization state is similar to that of a single isolated DNH system, as previously mentioned in Sec. 4. It should be noted that $x_1(0) = -0.5$, $x_2(0) = -0.51$, $y_1(0) = y_2(0) = 0$, and $z_1(0) = z_2(0) = 0$ are considered. Moreover, the output of variables x_1 (solid red line) and x_2 (cyan dashed line) are represented in Fig. 8, while other corresponding states are completely correlated and synchronized.

6. Conclusion

Studying linked circuits' synchronization state has emerged as a fascinating field of study due to its significant applicability in different fields, such as secure communication. The Chua system is a famous instance that is studied deeply in this field. This paper addresses the synchronization of another system proposed in [42] by adding a damping term to the third equation of the original conservative Nosé–Hoover system. The DNH system can exhibit a monostable attracting torus or a multistable one in coexistence with chaotic or periodic solutions. However, performing the bifurcation analysis, the paper focused on the chaotic monostable solution, which is significant in information processing. After determining the parameter settings, the equivalent analog circuit of the DNH system is implemented in the environment of OrCAD–PSpice, showing the expected output. Considering a passive resistor to link two circuits, the mathematical equations were expressed in diffusive form. Thereafter, the MSF analysis was performed to find out the coupling scheme leading to complete synchronization. The MSF-based results showed that the feedback term could result in synchronization in $1 \to 1$, $2 \to 2$, and $3 \to 3$ configurations, according to the notations in Tab. 1. Moreover, it was revealed that in the $3 \to 3$ configuration, when the normalized coupling parameter passed a threshold, the DNH systems maintained the synchronous behavior, while in the $1 \to 1$ scheme, this synchronous state can be detected in limited values of the normalized coupling parameter. On the other hand, when the $2 \to 2$ coupling scheme is considered, the synchronization was identified after the normalized coupling parameter crossed a threshold similar to case $3 \to 3$. However, before this threshold in small values of normalized coupling parameter, the synchronization was detected, similar to case $1 \to 1$. To confirm the results and to ensure that the results are attainable in real simulations, the synchronization error of two coupled circuits was computed. Finally, in each case, the equivalent circuits were designed, and the analog results delivered the synchronization of the two circuits.

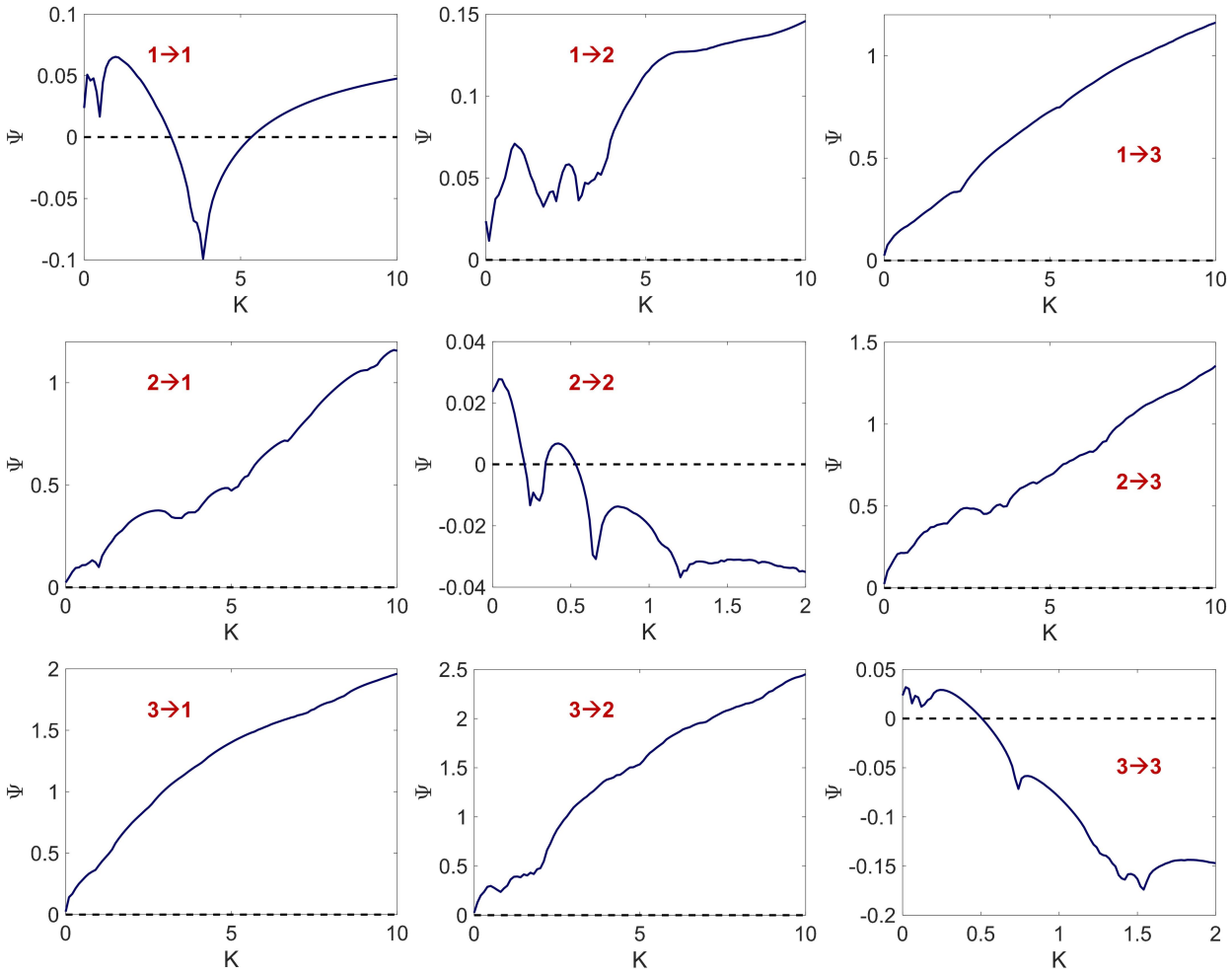

Fig. 5. The MSFs of the linearized variational equation with regard to the changes in the value of the normalized coupling parameter K. Here, different coupling schemes are considered and demonstrated with the same notation as in Tab. 1.

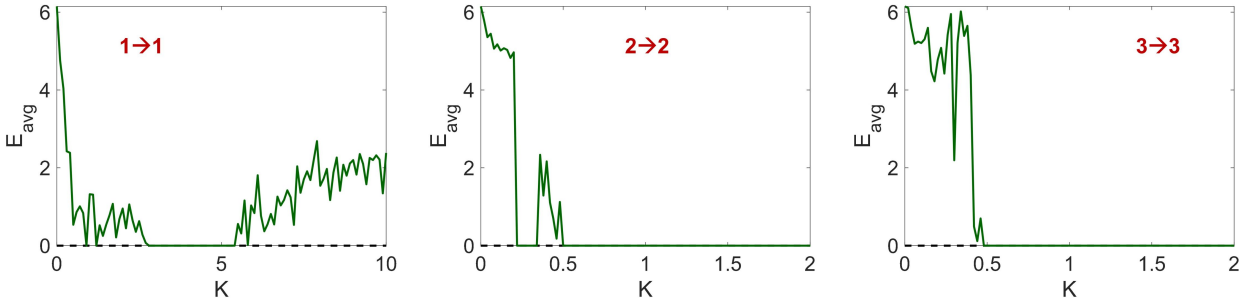

Fig. 6. The synchronization error of two diffusively coupled DNH systems with regard to the changes in the value of the normalized coupling parameter K. Here different coupling schemes (clarified in Systems (10)–(12) are considered and demonstrated with the same notation as in Tab. 1.

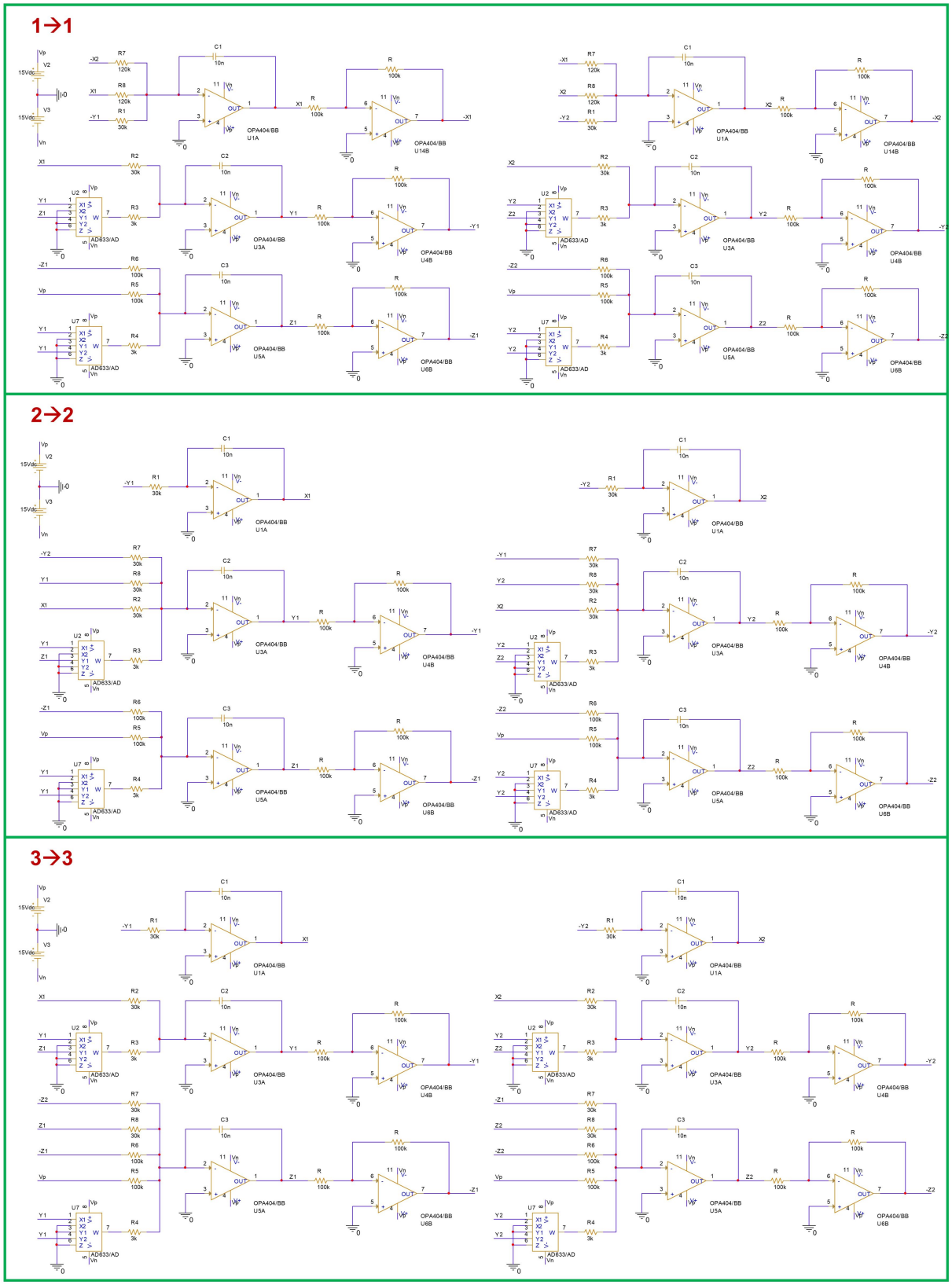

Fig. 7. The circuit implementation of two coupled DNH systems in the OrCAD–PSpice environment for $1 \rightarrow 1$, $2 \rightarrow 2$, $3 \rightarrow 3$ coupling schemes.

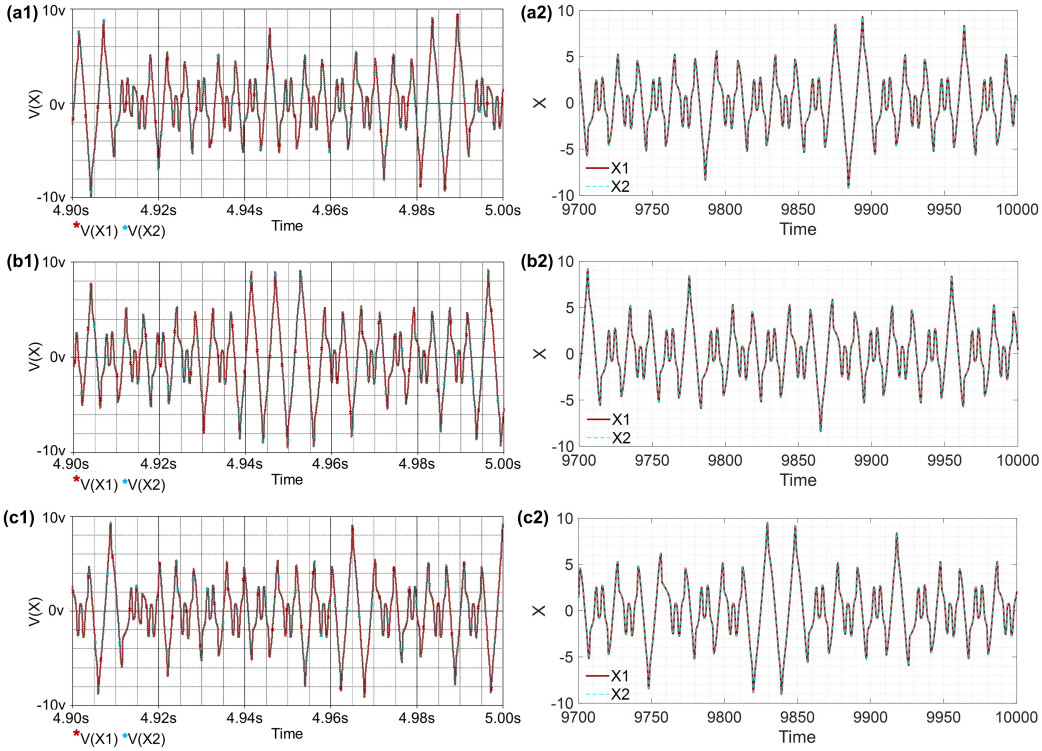

Fig. 8. The output (time series) of two coupled DNH systems in (a1), (a2) $1 \rightarrow 1$, (b1), (b2) $2 \rightarrow 2$, and (c1), (c2) $3 \rightarrow 3$ configurations. The first column contains the results obtained from OrCAD–PSpice for 5000 milliseconds, and the second column contains the results obtained from the MATLAB software for 10000 milliseconds. Here $x_1(0) = -0.5$, $x_1(0) = -0.51$, and $y_1(0) = y_2(0) = z_1(0) = z_2(0) = 0$ are considered.

Acknowledgments

Funded in part by the Natural Science Foundation of Changzhou College of Information Technology, China, under Grant CXZK202102Y.

References

[1] PETRZELA, J. Canonical hyperchaotic oscillators with single generalized transistor and generative two-terminal elements. *IEEE Access*, 2022, vol. 10, p. 90456–90466. DOI: 10.1109/ACCESS.2022.3201870

[2] PETRZELA, J. Hyperchaotic self-oscillations of two-stage class C amplifier with generalized transistors. *IEEE Access*, 2021, vol. 9, p. 62182–62194. DOI: 10.1109/ACCESS.2021.3074367

[3] PETRZELA, J., KOLKA, Z., HANUS, S. Simple chaotic oscillator: From mathematical model to practical experiment. *Radioengineering*, 2006, vol. 15, no. 1, p. 6–11. ISSN: 1210-2512

[4] SPROTT, J. C., THIO, W. J.-C. *Elegant Circuits: Simple Chaotic Oscillators*. World Scientific, 2021. ISBN: 9789811240010

[5] PETRZELA, J., HRUBOS, Z., GOTTHANS, T. Modeling deterministic chaos using electronic circuits. *Radioengineering*, 2011, vol. 20, no. 2, p. 438–444. ISSN: 1210-2512

[6] ORAVEC, J., TURAN, J., OVSENIK, L., et al. Asymmetric image encryption approach with plaintext-related diffusion. *Radioengineering*, 2018, vol. 27, no. 1, p. 281–288. DOI: 10.13164/re.2018.0281

[7] BERNSTEIN, G. M., LIEBERMAN, M. A. Secure random number generation using chaotic circuits. *IEEE Transactions on Circuits and Systems*, 1990, vol. 37, no. 9, p. 1157–1164. DOI: 10.1109/31.57604

[8] LIN, H., WANG, C., YU, F., et al. A review of chaotic systems based on memristive Hopfield neural networks. *Mathematics*, 2023, vol. 11, no. 6, p. 1–18. DOI: 10.3390/math11061369

[9] MA, X., WANG, C. Hyper-chaotic image encryption system based on N + 2 ring Joseph algorithm and reversible cellular automata. *Multimedia Tools and Applications*, 2023, p. 1–26. DOI: 10.1007/s11042-023-15119-0

[10] ZHU, Y., WANG, C., SUN, J., et al. A chaotic image encryption method based on the artificial fish swarms algorithm and the DNA coding. *Mathematics*, 2023, vol. 11, no. 3, p. 1–18. DOI: 10.3390/math11030767

[11] MA, X., WANG, C., QIU, W., et al. A fast hyperchaotic image encryption scheme. *International Journal of Bifurcation and Chaos*, 2023, vol. 33, no. 5, p. 1–21. DOI: 10.1142/S021812742350061X

[12] KUZNETSOV, N., MOKAEV, T., PONOMARENKO, V., et al. Hidden attractors in Chua circuit: Mathematical theory meets physical experiments. *Nonlinear Dynamics*, 2023, vol. 111, no. 6, p. 5859–5887. DOI: 10.1007/s11071-022-08078-y

[13] WANG, J., XIAO, L., RAJAGOPAL, K., et al. Fractional-order analysis of modified Chua's circuit system with the smooth degree of 3 and its microcontroller-based implementation with analog circuit design. *Symmetry*, 2021, vol. 13, no. 2, p. 5859–5887. DOI: 10.3390/sym13020340

[14] BAO, B., LI, Q., WANG, N., et al. Multistability in Chua's circuit with two stable node-foci. *Chaos: An Interdisciplinary Journal of Nonlinear Science*, 2016, vol. 26, no. 4, p. 1–9. DOI: 10.1063/1.4946813

[15] CHEN, M., LI, M., YU, Q., et al. Dynamics of self-excited attractors and hidden attractors in generalized memristor-based Chua's circuit. *Nonlinear Dynamics*, 2015, vol. 81, no. 1, p. 215–226. DOI: 10.1007/s11071-015-1983-7

[16] XU, Q., LIN, Y., BAO, B., et al. Multiple attractors in a non-ideal active voltage-controlled memristor based Chua's circuit. *Chaos, Solitons & Fractals*, 2016, vol. 83, p. 186–200. DOI: 10.1016/j.chaos.2015.12.007

[17] GUO, M., YANG, W., XUE, Y., et al. Multistability in a physical memristor-based modified Chua's circuit. *Chaos*, 2019, vol. 29, no. 4, p. 1–13. DOI: 10.1063/1.5089293

[18] YE, X., WANG, X., GAO, S., et al. A new chaotic circuit with multiple memristors and its application in image encryption. *Nonlinear Dynamics*, 2020, vol. 99, no. 2, p. 1489–1506. DOI: 10.1007/s11071-019-05370-2

[19] WANG, X., PHAM, V. T., JAFARI, S., et al. A new chaotic system with stable equilibrium: From theoretical model to circuit implementation. *IEEE Access*, 2017, vol. 5, p. 8851–8858. DOI: 10.1109/ACCESS.2017.2693301

[20] AHMADI, A., RAJAGOPAL, K., ALSAADI, F. E., et al. A novel 5D chaotic system with extreme multi-stability and a line of equilibrium and its engineering applications: Circuit design and FPGA implementation. *Iranian Journal of Science and Technology, Transactions of Electrical Engineering*, 2020, vol. 44, no. 1, p. 59–67. DOI: 10.1007/s40998-019-00223-5

[21] XU, Q., WANG, Y., CHEN, B., et al. Firing pattern in a memristive Hodgkin–Huxley circuit: Numerical simulation and analog circuit validation. *Chaos, Solitons & Fractals*, 2023, vol. 172, p. 1–10. DOI: 10.1016/j.chaos.2023.113627

[22] XU, Q., WANG, Y., IU, H. H. C., et al. Locally active memristor-based neuromorphic circuit: Firing pattern and hardware experiment. *IEEE Transactions on Circuits and Systems I: Regular Papers*, 2023, vol. 70, no. 8, p. 1–2. DOI: 10.1109/TCSI.2023.3276983

[23] BOCCALETTI, S., KURTHS, J., OSIPOV, G., et al. The synchronization of chaotic systems. *Physics Reports*, 2002, vol. 366, no. 1–2, p. 1–101. DOI: 10.1016/S0370-1573(02)00137-0

[24] ZHENG, Z., HU, G. Generalized synchronization versus phase synchronization. *Physical Review E*, 2000, vol. 62, no. 6, p. 7882–7885. DOI: 10.1103/PhysRevE.62.7882

[25] BELYKH, V. N., OSIPOV, G. V., PETROV, V. S., et al. Cluster synchronization in oscillatory networks. *Chaos: An Interdisciplinary Journal of Nonlinear Science*, 2008, vol. 18, no. 3, p. 1–6. DOI: 10.1063/1.2956986

[26] ROSENBLUM, M. G., PIKOVSKY, A. S., KURTHS, J. Phase synchronization of chaotic oscillators. *Physical Review Letters*, 1996, vol. 76, no. 11, p. 1804–1807. DOI: 10.1103/PhysRevLett.76.1804

[27] ROSENBLUM, M. G., PIKOVSKY, A. S., KURTHS, J. From phase to lag synchronization in coupled chaotic oscillators. *Physical Review Letters*, 1997, vol. 78, no. 22, p. 4193–4196. DOI: 10.1103/PhysRevLett.78.4193

[28] PARASTESH, F., JAFARI, S., AZARNOUSH, H., et al. Chimeras. *Physics Reports*, 2021, vol. 898, p. 1–114. DOI: 10.1016/j.physrep.2020.10.003

[29] BOCCALETTI, S., PISARCHIK, A. N., GENIO, C. I., et al. *Synchronization: From Coupled Systems to Complex Networks*. Cambridge University Press, 2018. ISBN: 9781107056268

[30] HUSSAIN, I., JAFARI, S., GHOSH, D., et al. Synchronization and chimeras in a network of photosensitive FitzHugh–Nagumo neurons. *Nonlinear Dynamics*, 2021, vol. 104, no. 3, p. 2711–2721. DOI: 10.1007/s11071-021-06427-x

[31] GHOSH, D., BANERJEE, S., CHOWDHURY, A. R. Synchronization between variable time-delayed systems and cryptography. *Europhysics Letters*, 2007, vol. 80, no. 3, p. 1–6. DOI: 10.1209/0295-5075/80/30006

[32] BANERJEE, S. *Chaos Synchronization and Cryptography for Secure Communications: Applications for Encryption*. Information Science Reference, 2010. ISBN: 9781615207381

[33] ZHOU, L., TAN, F., LI, X., et al. A fixed-time synchronization-based secure communication scheme for two-layer hybrid coupled networks. *Neurocomputing*, 2021, vol. 433, p. 131–141. DOI: 10.1016/j.neucom.2020.12.033

[34] FAN, W., WU, H., LI, Z., et al. Synchronization and chimera in a multiplex network of Hindmarsh–Rose neuron map with flux-controlled memristor. *The European Physical Journal Special Topics*, 2022, vol. 231, no. 22, p. 4131–4141. DOI: 10.1140/epjs/s11734-022-00720-5

[35] RAKSHIT, S., RAY, A., BERA, B. K., et al. Synchronization and firing patterns of coupled Rulkov neuronal map. *Nonlinear Dynamics*, 2018, vol. 94, no. 2, p. 785–805. DOI: 10.1007/s11071-018-4394-8

[36] PARASTESH, F., MEHRABBEIK, M., RAJAGOPAL, K., et al. Synchronization in Hindmarsh–Rose neurons subject to higher-order interactions. *Chaos: An Interdisciplinary Journal of Nonlinear Science*, 2022, vol. 32, no. 1, p. 1–11. DOI: 10.1063/5.0079834

[37] XU, Q., LIU, T., DING, S., et al. Extreme multistability and phase synchronization in a heterogeneous bi-neuron Rulkov network with memristive electromagnetic induction. *Cognitive Neurodynamics*, 2023, vol. 17, no. 3, p. 755–766. DOI: 10.1007/s11571-022-09866-3

[38] PECORA, L. M., CARROLL, T. L. Master stability functions for synchronized coupled systems. *Physical Review Letters*, 1998, vol. 80, no. 10, p. 2109–2112. DOI: 10.1103/PhysRevLett.80.2109

[39] BUSCARINO, A., FORTUNA, L., FRASCA, M., et al. Chua's circuits synchronization with diffusive coupling: New results. *International Journal of Bifurcation and Chaos*, 2009, vol. 19, no. 9, p. 3103–3107. DOI: 10.1142/S0218127409024670

[40] LU, R., RAMAKRISHNAN, B., FALAH, M. W., et al. Synchronization and different patterns in a network of diffusively coupled elegant Wang–Zhang–Bao circuits. *The European Physical Journal Special Topics*, 2022, vol. 231, no. 22, p. 3987–3997. DOI: 10.1140/epjs/s11734-022-00690-8

[41] MISHKOVSKI, I., MIRCHEV, M., CORINTO, F., et al. Synchronization analysis of networks of identical and nearly identical Chua's oscillators. In *IEEE International Symposium on Circuits and Systems (ISCAS)*. Seoul (South Korea), 2012, p. 2115–2118. DOI: 10.1109/ISCAS.2012.6271703

[42] CAO, B., WANG, Y.-F., WANG, L., et al. Cluster synchronization in complex network of coupled chaotic circuits: An experimental study. *Frontiers of Physics*, 2018, vol. 13, no. 5, p. 1–11. DOI: 10.1007/s11467-018-0775-1

[43] GAMBUZZA, L. V., FRASCA, M., GÓMEZ-GARDEÑES, J. Intralayer synchronization in multiplex networks. *Europhysics Letters*, 2015, vol. 110, no. 2, p. 1–6. DOI: 10.1209/0295-5075/110/20010

[44] BURBANO-L, D. A., YAGHOUTI, S., PETRARCA, C., et al. Synchronization in multiplex networks of Chua's circuits: Theory and experiments. *IEEE Transactions on Circuits and Systems I: Regular Papers*, 2020, vol. 67, no. 3, p. 927–938. DOI: 10.1109/TCSI.2019.2955972

[45] JAFARI, S., SPROTT, J. C., DEHGHAN, S. Categories of conservative flows. *International Journal of Bifurcation and Chaos*, 2019, vol. 27, no. 2, p. 1–16. DOI: 10.1142/S0218127419500214

[46] MEHRABBEIK, M., JAFARI, S., SPROTT, J. C. A simple three-dimensional quadratic flow with an attracting torus. *Physics Letters A*, 2022, vol. 451, p. 1–8. DOI: 10.1016/j.physleta.2022.128427

[47] WOLF, A., SWIFT, J. B., SWINNEY, H. L., et al. Determining Lyapunov exponents from a time series. *Physica D: Nonlinear Phenomena*, 1985, vol. 16, no. 3, p. 285–317. DOI: 10.1016/0167-2789(85)90011-9

[48] HUANG, L., CHEN, Q., LAI, Y.-C., et al. Generic behavior of master-stability functions in coupled nonlinear dynamical systems. *Physical Review E*, 2009, vol. 80, no. 3, p. 1–11. DOI: 10.1103/PhysRevE.80.036204

About the Authors ...

Rending LU received his B.S. and M.S. degrees in 2004 and 2007, respectively, from the Automotive Electronics Department, South China University of Technology, China. From 2008 to 2010, he was engaged in the design of automobile electronic control systems. In 2011, he returned to academia and joined the School of Electronic Engineering, Changzhou College of Information Technology, China. His general research interests are in the area of chaotic circuit design and modeling, chaotic secure communication, and chaotic dynamical system. He designed a variety of chaotic circuits suitable for automotive electronic control systems and obtained a number of Chinese invention patents. In particular, his current research focuses on chaotic secure communication for intelligent connected vehicles.

Hayder NATIQ received his B.S. and M.S. degrees from the Department of Applied Sciences, University of Technology, Baghdad, Iraq, in 2009 and 2014, respectively. He earned his Ph.D. degree from the University Putra Malaysia (UPM) in 2019. Currently, he serves as a senior lecturer in the College of Information Technology at Imam Ja'afar Al-Sadiq University in Baghdad, Iraq. His research interests include chaotic systems, chaos-based applications, and multimedia security.

Ahmed M. Ali ALI received a B.Eng. degree in Electrical Engineering from the University of Babylon, Babylon, Irqa, in 2012, a master's degree in Electronics and Communication Engineering from the University of Babylon, and a Ph.D. degree in Electrical Engineering-Biomedical Engineering from the University of Basrah, Basrah, Iraq, in 2014 and 2020, respectively. He is currently the head of the Electronics Department at AL-Furat AL-Awsat Technical University/ Technical Institute of Babylon. His research interests include chaos and circuit theory, biomedical concepts, cellular nonlinear networks (CNNs), mathematical modeling, electronics and communications, wireless sensor networks (WSNs), IOT engineerings and techniques and reaction-diffusion CNNs. He has two patents in the above-mentioned fields.

Hamid Reza ABDOLMOHAMMADI was born in Khomein, Iran. He received the B.Sc. degree from the Amirkabir University of Technology, Tehran, Iran, in 2005 and the M.Sc. and Ph.D. degrees from the Iran University of Science and Technology, Tehran, Iran, in 2008 and 2014, respectively, all in Power Electrical Engineering. He is currently a faculty member in the Department of Electrical and Electronic Engineering at Golpayegan College of Engineering, Isfahan University of Technology. His research interests include power system optimization, smart power grids, artificial intelligence, and nonlinear and chaotic systems.

Sajad JAFARI (corresponding author) was born in Kermanshah, Iran, in 1983. He received his BSc, MSc, and Ph.D. degrees in Biomedical Engineering in 2005, 2008, and 2013 from the Biomedical Engineering Department, Amirkabir University of Technology (Tehran Polytechnic), Tehran, Iran. He is currently an assistant professor there (since 2013). His research interests include nonlinear and chaotic systems and signals and mathematical biology. He is also interested in complex networks and collective behaviors in them, such as synchronization, Chimera states, and spiral waves. He serves as editor in the International Journal of Bifurcation and Chaos, International Journal of Electronics and Communications, and Radioengineering. He has been one of the highly cited researchers in 2019 and 2020, according to Clarivate Analytics. He also has won the COMSTECH award in mathematics (2019).